Chiang Mai J. Sci. 2018; 45(4) : 1985-1994
http://epg.science.cmu.ac.th/ejournal/
Contributed Paper

Comparative Studies on Energetic TATB and TATB/F_{2314}: From Theory to Experiment

Xilin Yan [a], Guozheng Zhao* [b,c], Wei Tang [a] and Mingfeng Tang [a]

[a] Institute of Chemical Materials, China Academy of Engineering Physics, Mianyang, 621999, PR China.

[b] School of Chemistry and Material Science, Shanxi Normal University, Linfen, 041004, PR China.

[c] College of Pharmacy, Purdue University, West Lafayette, 47907, USA.

* Author for correspondence; e-mail: zhaoguozheng99@126.com

Received: 15 January 2017
Accepted: 10 April 2017

ABSTRACT

1,3,5-Triamino-2,4,6-trinitrobenzene (TATB) crystal was examined by density functional theory (DFT) calculations. Molecular dynamics (MD) method was used to investigate TATB-based polymer-bonded explosive (PBX) with fluorine containing polymer F_{2314}. The elastic constants and mechanical properties (tensile modulus, bulk modulus, shear modulus, Poission ratio, etc) were reported for the TATB-based PBXs on different crystalline surfaces. The mechanical properties for TATB (100)/F_{2314} were evaluated at different temperatures. The mechanical properties of TATB/F_{2314} interface based on tensile-shear test were performed in different loading angles. The results show that electronic properties, including electronic and nuclear Fukui functions, provided a fundamental understanding of the electronic structure of TATB crystal. The mechanical properties of TATB can be effectively improved by the addition of small amounts of fluorine polymer F_{2314}. TATB/F_{2314} deforms more easily with the increasing temperatures. The coupled stress of interface under different loading angles is gradually decreasing.

Keywords: TATB, PBX, molecular dynamics, mechanical property, tensile-shear test

1. INTRODUCTION

TATB (1, 3, 5-Triamino-2, 4, 6-trinitrobenzene), an outstanding representative of nitro explosives [1,2], has been widely and extensively used in many fields of energetic materials in the past several decades [3]. The strong intramolecular and intermolecular hydrogen interactions in TATB lead to exceptional insensitivity to thermal, impact, friction, and shock insults, making it one of the most insensitive explosives [4,5]. TATB-based polymer-bonded explosive (PBX) is also the known insensitive high explosive [6]. The key problem of making PBX is how to choose a polymer with high strength and good adhesive to the base explosives. In general, the fluoropolymer, a random copolymer of chlorotrifluoroethylene (CTFE) and vinylidene difluoride (VDF), was widely used as the polymeric binder of the TATB-based PBX due to its thermal and chemical stability, good mechanical properties and strong electrophilic character of its fluorine atoms [7].

Up to date, a number of theoretical studies [8-10] and experimental measurements [11-13] have paid attention to the TATB and TATB-based PBXs. Wu *et al.* studied the electronic structure of the energetic crystalline solid TATB to examine the insulator-to-metal transition [14]. Density functional theory was employed by Fedorov *et al.* to investigate the structural and electronic properties of the TATB under the hydrostatic pressure of 0-40 GPa [15]. Classical molecular dynamics (MD) calculations were performed to reveal the effect of high pressure on the crystal structure of TATB [16]. Perger *et al.* present preliminary results on the structural and mechanical properties of TATB as obtained by ab-initio calculations [17]. Rykounov *et al.* systematically studied the influence of pressure on the thermodynamic, structural, and elastic properties of TATB molecular crystal [18].

TATB lattice parameters were measured by Yeager *et al.* using neutron diffraction during thermal cycling of loose powder and a pressed pellet [19]. X-ray powder diffraction at high pressures was used by Dattelbaum *et al.* to determine a hydrostatic compression curve for TATB from ambient pressure to 13.0 GPa [20]. The isothermal linear and volume compressions of TATB were determined from X-ray diffraction patterns by Cady *et al.* taken at hydrostatic pressures up to 10 GPa [21]. Three-point bending creep behaviors of TATB-based PBX and its styrene copolymer modified formulation were studied by Lin *et al.* to investigate the effects of binder component on the creep properties of PBX [22]. A tension-shear work holder with 7 loading angles, which can realize different loading states including pure tension, shear and coupled tension-shear, was devised by Tang *et al.* to investigate the mechanical properties of explosive crystal/binder interface in TATB-based PBX [23].

In this work, electronic and nuclear Fukui functions were calculated and analyzed to provide new insight into understanding of the electronic structure of TATB crystal. Meanwhile, mechanical properties of TATB-based fluorine-polymer (F_{2314}) PBX at 318K were reported from MD simulation, where F_{2314} are copolymers of VDF and CTFE with the molar ratios of 1:4. In addition, a systematic study on mechanical properties for TATB (100)/F_{2314} at different temperatures was also conducted. Finally, tensile-shear experiment was tested in different loading angles at 45°C 4MPa. Our study may provide basic information for theoretical and experimental studies on energetic TATB and TATB/F_{2314}.

2. MATERIALS AND METHODS

2.1 DFT Calculation

The crystal structure of TATB (reference code of TATNBZ from the Cambridge Structural Database, a = 9.010 Å, b = 9.028 Å, c = 6.812 Å, α = 108.58°, β = 91.82°, γ= 119.97°, figure 1) [24] was optimized with the lattice parameters held constant. Electronic perturbations to the optimized crystal structure were initiated by adding or removing one electron from the unit cell to calculate nucleophilic and electrophilic Fukui functions. B3LYP exchange-correlation functional [25] and 6-21G(d) basis set were selected for the calculations. The structural optimization and electronic calculation were conducted with a periodic quantum mechanical program, Crystal 09 [26]. The energy convergence of the optimization and energy calculations was set to 10^{-7} hartree. Electronic structure and properties calculated were visualized with OpenDX [27].

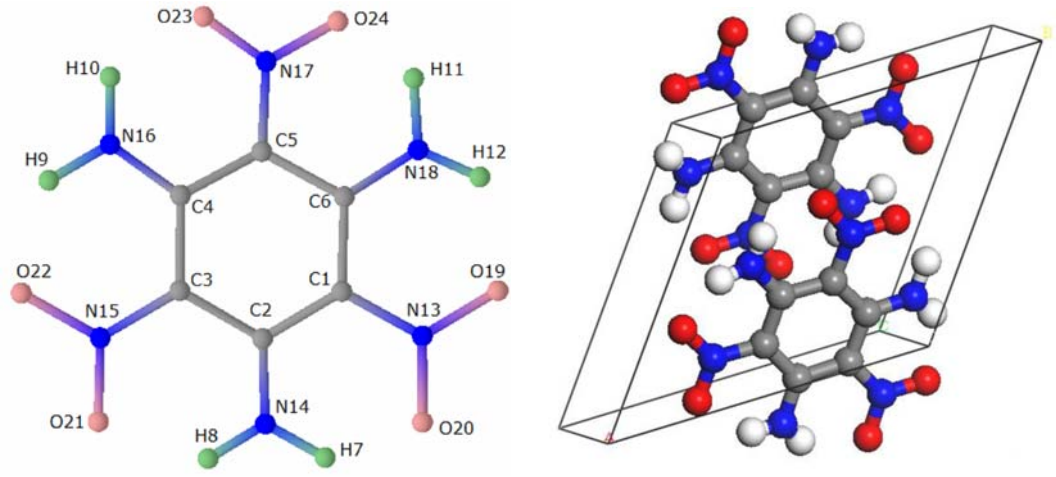

Figure 1. Molecular and crystal structures of TATB.

The electronic Fukui function (EFF), $f(r)$, is defined as the change in electron density, $r(r)$, upon the change in the total number of electrons, N, at constant external potential v [28,29]:

$$f(r) = \left(\frac{\partial \rho(r)}{\partial N}\right)_v \quad (1)$$

The number of electrons, N, in a molecule can be changed by an integer, the electronic Fukui function, $f(r)$ is resolved into nucleophilic $f^+(r)$ and electrophilic $f^-(r)$ components as shown in Equations (2) and (3), respectively:

$$f^+(r) = r^+(r) - r^0(r) \quad (2)$$

$$f^-(r) = r^0(r) - r^-(r) \quad (3)$$

In these equations, $r^+(r)$, $r^-(r)$, and $r^0(r)$ represent the electron densities of anionic, cationic, and neutral species of a given molecular system, respectively [28].

The electronic Fukui function can be further extended to the nuclear Fukui function (NFF), F_a, which is defined in Equation (4) [30,31]:

$$\mathbf{\Phi}_a = \left(\frac{\partial F_a}{\partial N}\right)_v \quad (4)$$

where F_a is dependent in part upon the molecular system's electronic structure; N is the number of electrons in the system and $v(r)$ is the external potential defined by nuclear charges. As such, the nuclear Fukui function concept can be further developed into nucleophilic and electrophilic components, numerically calculated by the finite differences [30,32]:

$$\mathbf{\Phi}^+_a = F^+_a - F^0_a \quad (5)$$

$$\mathbf{\Phi}^-_a = F^0_a - F^-_a \quad (6)$$

in which F^+_a, F^-_a, and F^0_a are the Hellmann-Feynman forces of the anionic, cationic, and neutral molecular systems, respectively.

2.2 MD Simulation

Pure TATB crystal and TATB-based PBXs were simulated by MD method with COMPASS force field. The force field was chosen because it can achieve a broad coverage with approximately the same level of quality [16]. The TATB supercell (4×3×4)

is cut along three crystalline surfaces (010), (100), and (001) with the "cutting" method as implemented in the commercial software Accelrys Materials Studio (MS) 6.0 [33]. Periodic supercells are separated from repeated replicas by 10 Å vacuum layer along the c (z) axis. F_{2314} (involving 10 chain segments) is processed by the Amorphous Cell module and simulated 2.5 ns with the MD method to get the equilibrium conformations. The end groups of F_{2314} chain are saturated by the H or F atoms according to their types. The equilibrium F_{2314} is embedded into the simulation box in parallel with different crystalline surfaces.

MD simulations are performed in the NVT ensemble with the COMPASS force field by the Discover module. The systems are first integrated for 2×10^5 time steps in all equilibration runs, which are necessary to attain the mechanical and thermal equilibrium, and then followed by the production runs of 1×10^5 time steps, during which data are collected for subsequent analysis. A fixed time step size of 1 fs is used in all cases. The Andersen thermostat method [34] is employed to control the system. The mechanical properties are estimated by the static mechanics method as implemented in the MS 6.0 program.

3. RESULTS AND DISCUSSION

3.1 Fukui Function

Fukui functions may describe the local polarizability that stem from electron sharing and mobility [35]. Illustrated in Figures 2 and 3 are the Fukui functions calculated for the TATB crystal. It is clearly shown that the $-NO_2$ group in TATB has the largest distribution of nucleophilic EFF, followed by C2, C4 and C6 (Figure 2a). The electrophilic EFFs have large distributions around the nitro group, part of the benzene skeleton (C3 and C5), N14 and N16 (Figure 2b). This may suggest that atoms H7, H8, H9, H10, H11 and H12 are less important in participating in the frontier orbitals of the molecule.

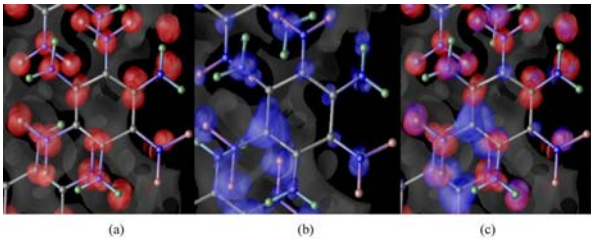

Figure 2. Electronic Fukui functions of TATB superimposed with isosurfaces of electron density (0.001 a.u.) in gray: (a) the nucleophilic (isosurface, 0.001 a.u.) in red, (b) the electrophilic (isosurface, 0.015 a.u.) in blue, and (c) both.

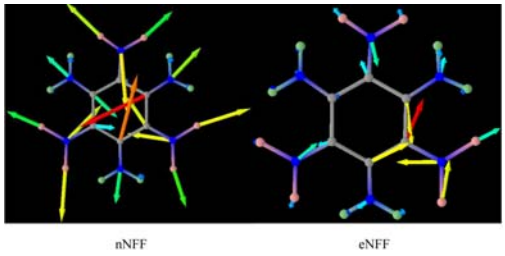

Figure 3. Vector representations of nucleophilic nuclear Fukui functions (nNFF, $\mathbf{\Phi}^+_a$ in nN), and electrophilic nuclear Fukui functions (eNFF, $\mathbf{\Phi}^-_a$ in nN) of TATB. Vector lengths (small to large) and colors (blue to red) represent relative magnitudes of the nuclear Fukui functions.

Table 1 lists the scales of nucleophilic nuclear Fukui functions (nNFF) and electrophilic nuclear Fukui functions (eNFF) calculated of the TATB crystal structure. Nuclear Fukui functions on C, O, and N atoms are much larger than those on H atoms. The largest values of Φ^+_a are on C2 and C6 (0.173 and 0.182 nN, respectively), and all of the H atoms have the smallest value. On the other hand, the largest values of Φ^-_a are on C1 and C6 (0.022 and 0.018 nN, respectively). Value on O22, H9 and H10 are smallest (0.002 nN). Scales of the NFFs, indicated by arrows in Figure 3, seem to correspond well with those of the EFFs, with the nitro group holding the largest values. C2 and C6 in TATB bear the larger distribution of nucleophilic EFFs as well as the larger corresponding nucleophilic NFFs. The results indicate that the NFFs closely match the EFFs and the largest nucleophilic NFFs value is about 8 times more than the largest electrophilic NFFs value. The study may shed light on utilizing the DFT concepts to understand the electronic structure of TATB crystal.

Table 1. Magnitudes of nucleophilic nuclear Fukui functions (Φ^+_a in nN) and electrophilic nuclear Fukui functions (Φ^-_a in nN) of TATB.

	C1	C2	C3	C4	C5	C6	H7	H8
Φ^+_a	0.121	0.173	0.053	0.083	0.023	0.182	0.017	0.007
Φ^-_a	0.022	0.017	0.006	0.003	0.007	0.018	0.004	0.002
	H9	H10	H11	H12	N13	N14	N15	N16
Φ^+_a	0.010	0.016	0.018	0.013	0.127	0.087	0.122	0.077
Φ^-_a	0.002	0.002	0.004	0.003	0.016	0.006	0.010	0.003
	N17	N18	O19	O20	O21	O22	O23	O24
Φ^+_a	0.147	0.109	0.132	0.096	0.128	0.092	0.115	0.093
Φ^-_a	0.010	0.007	0.010	0.016	0.004	0.002	0.005	0.004

3.2 Mechanical Properties for TATB Based PBXs at 318K

There are two criteria to judge the equilibrium of MD simulation: one is the equilibrium of temperature (i.e., the fluctuation of temperature is within 15 K) and another is the equilibrium of energy (i.e., the energy is invariable or has small fluctuation around the average energy value). According to the criteria, all simulated systems have basically reached balance. Table 2 summarizes the elastic constants C_{ij} of the TATB crystal and its PBXs on different crystalline surfaces at 318 K. Due to elastic strain energy, $C_{ij}=C_{ji}$ even for extremely anisotropic materials, the number of independent elastic coefficients was reduced to 21. Elastic modulus, measurement of rigidity, is the ratio of stress to strain.

Table 3 presents the mechanical properties, including tensile modulus (E), bulk modulus (K), shear modulus (G), ratio of bulk modulus and shear modulus (K/G), Poisson's ratio (γ), and Cauchy pressure (C_{12}-C_{44}) of TATB crystal and its PBXs on different crystalline surfaces at 318 K. Clearly, γ, K/G, and C_{12}-C_{44} of TATB (010)/F_{2314}, TATB (100)/F_{2314}, and TATB (001)/F_{2314} are comparable to or larger than those of pure TATB. Among the PBXs on different crystalline surfaces, TATB (001)/F_{2314} has the largest E, G and the smallest C_{12}-C_{44}; TATB (100)/F_{2314} possesses the second largest E and G, while the smallest K.

Table 2. Elastic constants (GPa) of the TATB crystal and its PBXs on different crystalline surfaces at 318 K.

Elastic constant (GPa)	TATB	TATB (010)/F_{2314}	TATB (100)/F_{2314}	TATB (001)/F_{2314}
C_{11}	40.4	8.4	16.7	18.6
C_{22}	34.7	16.1	7.3	19.2
C_{33}	27.3	10.0	9.0	7.2
C_{44}	13.8	1.8	1.0	8.0
C_{55}	1.7	2.0	3.1	0.9
C_{66}	1.2	3.3	1.1	0.9
C_{12}	8.8	4.1	3.3	3.9
C_{13}	2.6	4.6	2.8	2.6
C_{23}	3.3	3.2	4.0	2.6
C_{15}	0.5	0.0	-0.2	0.1
C_{25}	0.6	0.1	0.1	0.3
C_{35}	-0.2	-1.7	0.0	-0.1
C_{46}	-0.3	-0.8	0.05	-0.1

Table 3. Mechanical properties for TATB crystal and its PBXs on different crystalline surfaces at 318 K.

	TATB	TATB (010)/F_{2314}	TATB (100)/F_{2314}	TATB (001)/F_{2314}
Tensile modulus E (GPa)	37.3	5.7	15.6	17.2
Bulk modulus K (GPa)	8.8	4.4	3.4	4.0
Shear modulus G (GPa)	15.8	2.2	6.7	7.4
Poisson ratio γ	0.2	0.3	0.2	0.2
K/G	0.6	2.0	0.5	0.5
C_{12}-C_{44}	-5.0	2.3	2.3	-4.1

Table 4. Mechanical properties for TATB (100)/F_{2314} at different temperatures.

	278 K	298 K	318 K	338 K	358 K
Tensile modulus E (GPa)	15.9	15.7	15.6	15.9	15.5
Bulk modulus K (GPa)	3.5	3.4	3.4	3.1	3.2
Shear modulus G (GPa)	6.8	6.8	6.7	6.9	6.7
Poisson ratio γ	0.2	0.2	0.2	0.2	0.2
K/G	0.5	0.5	0.5	0.4	0.5
C_{12}-C_{44}	2.0	2.2	2.3	2.3	2.6

The larger the E a material has, the stronger the rigidity is [34]. C_{12}-C_{44} [35] is a criterion to evaluate the ductility and brittleness of a material. The positive value of C_{12}-C_{44} stands for a ductile material and the negative for a brittle material, and the more positive the value is, the more ductile the material is. According to these criteria, it can be known that the PBXs on different crystalline surfaces at 318 K has better tenacity and ductility

than TATB crystal, indicating that introduction of F_{2314} into TATB makes rigidity decrease while tenacity, malleability, and ductility increase. Comparing three PBXs, TATB (100)/F_{2314} has the best plastic property.

3.3 Mechanical Properties for TATB (100)/F_{2314}

The mechanical properties, including E, K, G, K/G, γ, and C_{12}-C_{44} of TATB (100)/F_{2314} at different temperatures are shown in Table 3. From the data in Table 3, the tensile modulus E decreases from 15.9 GPa to 15.5 GPa as the system changes from 278 K to 358 K, the bulk modulus K decreases from 3.5 GPa to 3.2 GPa, and the shear modulus G decreases slightly as compared to the former two moduli. This further indicates that the rigidity and brittleness of TATB (100)/F_{2314} decrease from 278 to 318 K, while the elasticity and plasticity strengthen. Meanwhile, these variations also suggest that the materials will deform more easily with the increasing temperatures, because the resistance to plastic deformation is proportional to the elastic shear modulus G and the fracture strength for materials is proportional to the bulk modulus K. Considering the content of F_{2314} in the simulated PBXs is about 5-10%, which is nearly equivalent to the percentage of a polymer in the actual PBXs, it is therefore concluded that the mechanical properties of TATB (100)/F_{2314} can be effectively improved by blending TATB with small amounts of F_{2314}. Commonly, the Poisson ratios of TATB (100)/F_{2314} from 278 K to 358 K are all 0.2. The quotient K/G is nearly unchanged in this temperature range, so that the ductility is almost the same. This is because the relative change rates of G and K are about the same with the increasing temperatures.

3.4 Tensile-shear Experimental Results in Different Loading Angles at 45°C 4MPa

By changing the loading angles, experimental test for mechanical properties of interface under 45°C 4MPa conditions was carried out, as shown in Figure 4, and Figure 5. The experimental results are as following: the coupled stress of interface under different loading angles is gradually decreasing; the decreasing amplitude under different loading angles is in the range of 2.16%~13.95%. The coupled stress is divided into tension stress in vertical interface direction and shear stress in parallel interface direction, and the corresponding tension/shear stress also trend to decrease, and decreasing amplitude is in the above ranges. There are differences between the aforementioned test results and traditional knowledge, which reflect as follows: traditional understanding acknowledged that the temperature increase during interface forming could enhance the fluidity of binder, therefore, help to form an interface with stronger binding effect. But, the test results are contradiction. The reason for that is analyzed as following: during the interface forming, the base material is the polymer bonded explosive, and cannot be softened by a temperature of 45°C, and therefore be regarded as a rigid body to the binder. With the temperature decreases to a normal one after the interface formed, a strong internal stress in the parallel interface direction is bound to form owing to the rule that materials expand with heat and contract with cold. The internal stress may be the main reason for the experimental phenomenon.

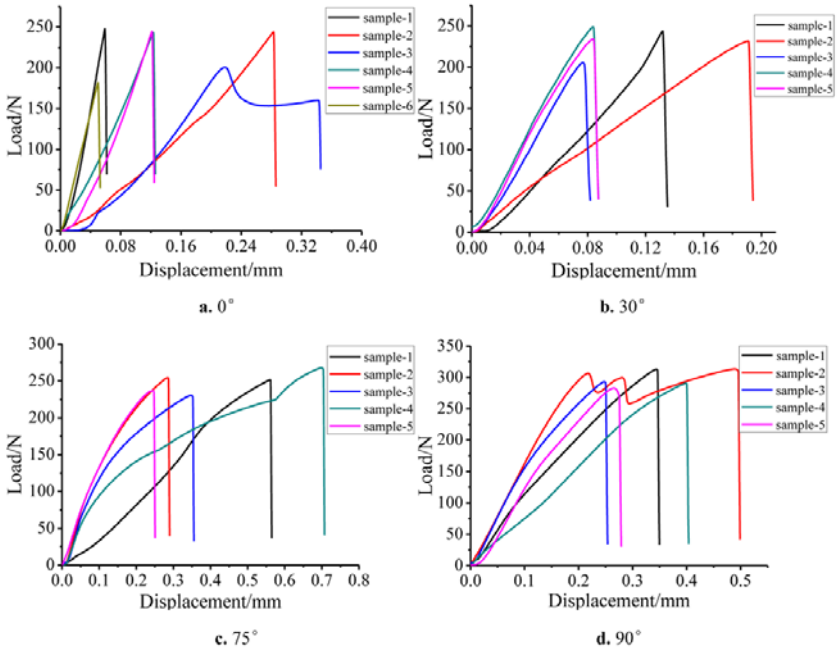

Figure 4. Tensile-shear experimental results in different loading angles at 45°C 4MPa.

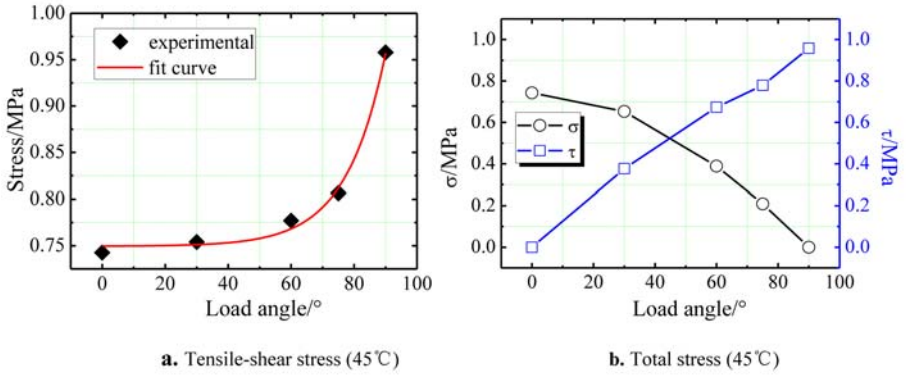

Figure 5. Relationships between the tensile-shear results and loading angles at 45°C 4MPa.

4. CONCLUSIONS

In this work, calculation of the electronic structure of TATB crystal and the analysis of Fukui functions have provided fundamental insight with regard to the local stability flexibility of molecular structure and the mutual connection to crystal packing. The mechanical properties of the crystal TATB can be effectively improved by the additions of small amounts of F_{2314}, and the effect of F_{2314} on the improvement of mechanical properties on three crystalline surfaces is that TATB (100)/F_{2314} has the best plastic property. TATB/F_{2314} deforms more easily from 278 K to 358 K. The coupled stress of interface under different loading angles is gradually decreasing, and the decreasing amplitude under different loading angles is in the range of 2.16%~13.95%.

ACKNOWLEDGMENTS

This work was supported by National Natural Science Foundation of China (No. 11302198), Scientific and Technologial

Innovation Programs of Higher Education Institutions in Shanxi (No. 2016157) and Undergraduate Training Program for Innovation and Entrepreneurship (No. WL2016CXCY-YJ-25). We were indebted to and thank Prof. Tonglei Li (Purdue University, USA) for many helpful support of our work.

REFERENCES

[1] Kroonblawd M.P. and Sewell T.D., *J. Phys. Chem. C*, 2016; **120**: 17214-17223. DOI 10.1021/acs.jpcc.6b04749.

[2] Yan Z.H., Zhang C.C., Yan H.W., Li Z.J., Li L., Huang M., Tan B.S. and Yuan X.D., *Adv. Cond. Matter Phys.*, 2014; 219547. DOI 10.1155/2014/219547.

[3] Naksawee A., Hayashi K. and Pananont P., *Chiang Mai J. Sci.*, 2016; **43**: 1269-1278.

[4] Wen Y.S., Zhang C.Y., Xue X.G. and Long X.P., *Phys. Chem. Chem. Phys.*, 2015; **17**: 12013-12022. DOI 10.1039/c5cp 00006h.

[5] Zhao G.Z., Jia J.F. and Wu H.S., *J. Chem. Sci.*, 2016; **128**: 1223-1236. DOI 10.1007/s12039-016-1117-x.

[6] Liu Y.R., Duan Z.P., Zhang Z.Y., Ou Z.C. and Huang F.L., *J. Hazard. Mater.*, 2016; **317**: 44-51. DOI 10.1016/j.jhazmat.2016. 05.052.

[7] Cady W.E. and Caley L.E., *Properties of Kel-F 800 Plymer*, Lawrence Livermore Laboratory Report, UCRL-52301, 1977.

[8] Bedrov D., Borodin O., Smith G.D., Sewell T.D., Dattelbaum D.M. and Stevens L.L., *J. Chem. Phys.*, 2009; **131**: 224703. DOI 10.1063/1.3264972.

[9] Budzevich M.M., Landerville A.C., Conroy M.W., Lin Y., Oleynik I.I. and White C.T., *J. Appl. Phys.*, 2010; **107**: 113524. DOI 10.1063/1.3361407.

[10] Gee R.H., Roszak S., Balasubramanian K. and Fried L.E., *J. Chem. Phys.*, 2004; **120**: 7059-7066. DOI 10.1063/1.1676120.

[11] Palmas P., Botzanowski T., Guerain M., Forzy A., Bruneton E. and Delrio G., *J. Phys. Chem. B*, 2016; **120**: 4152-4159. DOI 10.1021/acs.jpcb.6b02176.

[12] Burtsev V.V., Komrachkov V.A., Kovtun A.D., Panov K.N., Rudnev A.V. and Syrunin M.A., *Combust. Explo. Shock+*, 2012; **48**: 343-349. DOI 10.1134/ S0010508212030124.

[13] Hooks D.E., Ramos K.J., Bolme C.A. and Cawkwell M.J., *Propellants Explos. Pyrotech.*, 2015; **40**: 333-350. DOI 10.1002/prep.201400282.

[14] Wu C.J., Yang L.H., Fried L.E., Quenneville J. and Martinez T.J., *Phys. Rev. B*, 2003; **67**: 235101. DOI 10.1103/ PhysRevB.67.235101.

[15] Fedorov I.A. and Zhuravlev Y.N., *Chem. Phys.*, 2014; **436-437**: 1-7. DOI 10.1016/ j.chemphys.2014.03.013.

[16] Kohno Y., Mori K., Hiyoshi R.I., Takahashi O. and Ueda K., *Chem. Phys.*, 2016; **472**: 163-172. DOI 10.1016/j. chemphys.2016.04.002.

[17] Valenzano L., Slough W.J. and Perger W., *AIP Conference Proceedings: Shock Compression of Condensed Matter*, Springer-Verlag, 2012; **1426**: 1191-1194.

[18] Rykounov A.A., *J. Appl. Phys.*, 2015; **117**: 215901. DOI 10.1063/1.4921815.

[19] Yeager J.D., Luscher D.J., Vogel S.C., Clausen B. and Brown D.W., *Propellants Explos.*, 2016; **41**: 514-525. DOI 10.1002 /prep.201500286.

[20] Stevens L.L., Velisavljevic N., Hooks D.E. and Dattelbaum D.M., *Propellants Explos. Pyrotech.*, 2008; **33**: 286-295. DOI 10.1002/prep.200700270.

[21] Olinger B. and Cady H.H., *Proceeding of the 6th International Detonation Symposium*, Coronado, California, 1976; 700-709.

[22] Lin C.M., Liu J.H., Huang Z., Gong F.Y., Li Y.B., Pan L.P., Zhang J.H. and Liu S.J., *Propellants Explos. Pyrotech.*, 2015; **40**: 189-196. DOI 10.1002/prep.201400203.

[23] Yan X.L., Tang M.F., Gan H.X., Wang L., Li M. and Wen M.P., *Chin. J. Energ. Mater.*, 2016; **24**: 587-591. DOI 10.11943/j.issn.1006-9941.2016.06.013.

[24] Cady H.H. and Larson A.C., *Acta Crystallogr.*, 1965; **18**: 485-496. DOI 10.1107/S0365110X6500107x.

[25] Becke A.D., *J. Chem. Phys.*, 1993; **98**: 5648-5652. DOI 10.1063/1.464913.

[26] Dovesi R., Saunders V.R., Roetti C., Orlando R., Zicovich-Wilson C.M., Pascale F., Civalleri B., Doll K., Harrison N.M. and Bush I.J., *CRYSTAL09*, University of Torino, Torino, 2009.

[27] Thompson D., Braun J. and Ford R., *OpenDX: Paths to Visualization*, VIS Inc., Missoula, MT, 2000.

[28] Ayers P.W. and Levy M., *Theor. Chem. Acc.*, 2000; **103**: 353-360. DOI 10.1007/s002149900093.

[29] Parr R.G. and Yang W.T., *J. Am. Chem. Soc.*, 1984; **106**: 4049-4050. DOI 10.1021/ja00326a036.

[30] Cohen M.H., Ganduglia-Pirovano M.V. and Kudrnovsky J., *J. Chem. Phys.*, 1994; **101**: 8988-8997. DOI 10.1063/1.468026.

[31] Proft F.D., Liu S. and Geerlings P., *J. Chem. Phys.*, 1998; **108**: 7549-7554. DOI 10.1063/1.476188.

[32] Cohen M.H., Ganduglia-Pirovano M.V. and Kudrnovsky J., *J. Chem. Phys.*, 1995; **103**: 3543-3551. DOI 10.1063/1.470238.

[33] Materials Studio 6.0, Accelrys, 2012.

[34] Andersen H.C., *J. Chem. Phys.*, 1980; **72**: 2384-2393. DOI 10.1063/1.439486.

[35] Li T.L., Ayers P.W., Liu S.B., Swadley M.J. and Aubrey-Medendorp C., *Chem. Eur. J.*, 2009; **15**: 361-371. DOI 10.1002/chem. 200801056.